IOP PUBLISHING JOURNAL OF PHYSICS D: APPLIED PHYSICS

J. Phys. D: Appl. Phys. **42** (2009) 195103 (6pp) doi:10.1088/0022-3727/42/19/195103

High photocarrier mobility in ultrafast ion-irradiated $In_{0.53}Ga_{0.47}As$ for terahertz applications

J C Delagnes[1], P Mounaix[1], H Němec[2], L Fekete[2], F Kadlec[2], P Kužel[2,4], M Martin[3] and J Mangeney[3]

[1] Centre de Physique Moléculaire Optique et Hertzienne, CNRS, UMR 5798, 351 Cours de la libération, 33405 Talence Cedex, France

[2] Institute of Physics, Academy of Sciences of the Czech Republic, Na Slovance 2, 182 21 Prague 8, Czech Republic

[3] Institut d'Electronique Fondamentale, CNRS, UMR 8622, Université Paris XI, 91405 Orsay Cedex, France

E-mail: kuzelp@fzu.cz

Received 25 June 2009, in final form 1 August 2009
Published 14 September 2009
Online at stacks.iop.org/JPhysD/42/195103

Abstract

Optical pump–terahertz (THz) probe spectroscopy was used for investigation of electron dynamics in $In_{0.53}Ga_{0.47}As$ films irradiated by heavy ions (Br^+) at doses from 10^9 to 10^{12} cm^{-2}. From the transient conductivity spectra, photoexcited electron lifetimes and mobilities were determined; their decrease is observed upon increase in the irradiation dose. At the highest dose, the material combines an electron lifetime of 0.46 ps with an exceptionally high photoexcited electron mobility of 3600 cm^2 V^{-1} s^{-1}. This last value is even higher than those reported for low-temperature-grown GaAs with similar electron lifetime. Due to its rather low band gap, heavy-ion irradiated $In_{0.53}Ga_{0.47}As$ shows promising properties for the development of THz systems using telecommunication based technology.

(Some figures in this article are in colour only in the electronic version)

1. Introduction

The generation of pulsed coherent terahertz (THz) radiation in photoconductive antennas [1] is most frequently achieved by optical excitation at ~800 nm with Ti : sapphire based sources. Usually, photoswitch antennas are made of low-temperature-grown (LTG) GaAs that combine sub-picosecond carrier lifetime, high photocarrier mobility and high dark electrical resistivity. Nevertheless, with the recent advent of compact, low cost and stable fibre lasers operating at ~1.5 μm, it is now highly desirable to develop THz emitters and detectors with band gap energy below 0.8 eV directly excited at this particular wavelength [2].

To engineer such materials, many technological efforts have been made, including the use of $In_{0.53}Ga_{0.47}As$ (InGaAs) with ion implantation [3] or of LTG InGaAs [4]. Although the ion-implanted InGaAs exhibits sub-picosecond carrier lifetime, its dark resistivity and Hall mobility reported so far are not very high [5] and, unlike in LTG GaAs, it is difficult to achieve high resistivity and ultrafast response simultaneously in LTG InGaAs [4]. Recently a picosecond photocarrier response was demonstrated in InGaAs with embedded ErAs nanoislands [6]. In contrast to low-temperature growth and ion implantation, the high-energy heavy-ion-irradiation technique mainly produces displacements of clusters of host atoms in the region of interest, allows a large tunability of optoelectronic properties of the damaged material and provides considerable flexibility in the design [7]. In particular, with the ion-irradiation technique, the carrier lifetime in InGaAs material can be reduced down to 300 fs with no decrease in the dark resistivity [8].

Ion-irradiated InGaAs samples were recently tested as THz emitters and detectors excited at either 800 or 1.55 μm; however, these experiments provided only little insight into the

[4] Author to whom any correspondence should be addressed.

ultrafast properties of InGaAs [9, 10]. Detailed information on ultrafast photocarrier response can be learned from time-resolved THz experiments [11, 12]. Namely, this technique yields a material parameter determining the efficiency of ultrafast optoelectronic devices, the transient mobility of photocarriers.

In this paper, we report on optical pump–THz probe measurements in a series of InGaAs films irradiated with different Br^+ ion doses. From the experimental results we deduce photoexcited electron behaviour on the ultrafast timescale depending on the irradiation dose.

2. Experimental details

The samples consist of initially undoped 3 μm thick $In_{0.53}Ga_{0.47}As$ layers epitaxially grown by gas-source molecular-beam epitaxy on semi-insulating InP : Fe substrates. The layers were subsequently irradiated by 11 MeV Br^+ ions at irradiation doses of 1×10^9, 1×10^{10}, 1×10^{11} and 1×10^{12} cm^{-2} (samples denoted as A, B, C and D, respectively).

Damage profiles across the InGaAs layer were estimated using the 'Stopping Range of Ions in the Matter' (SRIM) software [13]. Due to the very high initial energy of the incident ions, the InGaAs layer is practically free of bromine used for the bombardment, and the lattice damage is here solely due to host-atom displacements (cf figure 1 in [11]). Considering the irradiation dose used in the experiments, the density of the defects n_{host} is expected to be proportional to the irradiation dose (e.g. at the surface of the D sample, $n_{host} \approx 2\times10^{19}$ cm^{-3}). It was previously shown that the heavy ion-irradiation process (Br^+, Au^+) creates in majority defect clusters and some few point defects [14]. These extended defects have neutral charge and show deep energy levels [15], whereas the point defects are shallow ionized defects [16] with an activation energy value close to the one of the EL-2 like defect introduced by the low-temperature growth technique. All these defects act as traps and scattering and recombination centres for free carriers thus reducing their lifetime and momentum scattering time.

An optical pump–THz probe experimental setup (see [17] for a detailed description) was used to determine the transient THz transmission spectra. The amplified laser optical pulses with a 50 fs duration, 810 nm central wavelength and 1 mJ energy were provided by Ti : sapphire amplifier (Quantronix, Odin). The pulse train was split into three branches equipped with delay lines in order to adjust the arrival time of the pulses to the sample and to the sensor. The first branch was used for photoexcitation of the samples at 810 nm. The second branch was used for generation of THz pulses via optical rectification in a 1 mm thick [0 1 1] ZnTe crystal. The THz pulses were subsequently used for probing the ultrafast photoconductivity of the samples. The third branch served for the phase-sensitive detection of the transmitted THz field using a gated electro-optic detection scheme in another 1 mm thick [0 1 1] ZnTe crystal.

The pump and probe beam were sent collinearly to the sample in order to achieve a sub-picosecond time resolution (essentially limited by the detector responsivity [18]). Due to the short absorption length of InGaAs at 810 nm (~200 nm), free carriers are generated only in a surface layer free of implanted Br atoms. The pump fluence was kept relatively low (~1 μJ cm^{-2}) in order to limit the trap filling which leads to longer carrier lifetimes [11]. Initial photocarrier densities were 3.1×10^{17} cm^{-3} for samples A, B and C and 2.4×10^{17} cm^{-3} for sample D.

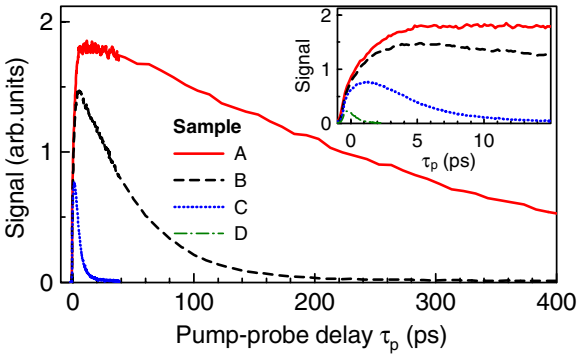

Figure 1. Pump–probe scans. Inset: initial 15 ps. (Colour online.)

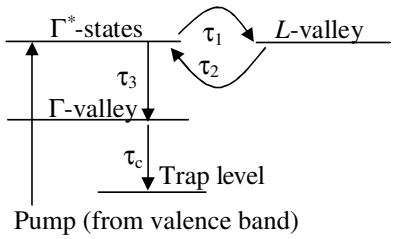

Figure 2. Energy level scheme considered to account for the intervalley scattering and the carrier trapping.

3. Results

Spectrally unresolved information about the charge dynamics can be obtained from pump–probe scans. To this end, the transient signal (corresponding to the maximum of the transient THz time-domain waveform) is recorded as a function of the pump–probe delay τ_p (figure 1). Since the hole mobility is considerably smaller than the electron mobility [19], we ascribe the observed signal to the response of electrons. Two regimes can be identified. (i) Immediately after the photoexcitation, a picosecond rise of the signal is observed for all samples (τ_{rise} = 1.9, 1.8 and 1.3 ps for samples A, B and C, respectively). (ii) The signal then decays due to the capture of electrons (the lifetimes are τ_c = 300 ps, 45 ps and 3.1 ps for samples A, B and C, respectively).

3.1. Intervalley scattering and carrier cooling

The excess energy of conduction band electrons immediately after photoexcitation at 810 nm is about 0.72 eV [19]. The initial picosecond rise of the transient THz signal then reflects an increase in the mobility due to the transfer of hot electrons between Γ and L valleys and due to their cooling [20, 21] (figure 2). Note that the progressive increase in the pump–probe signal cannot be achieved without considering a state

where the electron mobility is much smaller than that at the bottom of the Γ valley [21, 22]. This condition is fulfilled for carriers in the L-valley but not for hot electrons in the Γ valley (where the mobility is still not negligible). We developed a kinetic model which describes the variation of electron populations in distinct valleys of the conduction band and is able to account for the intervalley scattering phenomena observed in all samples. Similarly to Ralph *et al* [21], we assume that photoexcitation generates hot electrons in the Γ valley (denoted as Γ*). These either scatter to the L valley (τ_1) or relax to the bottom of the Γ valley (τ_3) where they can be captured with a characteristic time τ_c as shown in figure 2. From the L valley, electrons can scatter back to the Γ* state (τ_2). Resulting concentrations of Γ, Γ* and L electrons can be described by kinetic equations:

$$\frac{\mathrm{d}}{\mathrm{d}t}\begin{pmatrix} n_{\Gamma*} \\ n_{\mathrm{L}} \\ n_{\Gamma} \end{pmatrix} = \begin{pmatrix} -\left(\tau_1^{-1}+\tau_3^{-1}\right) & \tau_2^{-1} & 0 \\ \tau_1^{-1} & -\tau_2^{-1} & 0 \\ \tau_3^{-1} & 0 & -\tau_c^{-1} \end{pmatrix} \begin{pmatrix} n_{\Gamma*} \\ n_{\mathrm{L}} \\ n_{\Gamma} \end{pmatrix}, \tag{1}$$

and, finally, expressed as a combination of exponential functions with characteristic decay times T_x, T_y and T_z. The expression for these time constant eigenvalues can be derived analytically for the general case. One finds e.g. $T_z = \tau_c$ (carrier trapping); the other two eigenvalues are described by more complicated expressions. In the special case when $\tau_1 \ll \tau_2, \tau_3$ one obtains $T_x \approx \tau_1$ (initial transfer of the Γ* carriers into the L-valley which is not directly accessible in our experiments due to the limited time resolution), $T_y \approx \tau_3\tau_2/\tau_1$ (carrier cooling). As pointed out in [20], the ratio τ_2/τ_1 corresponds for long enough times after excitation to the ratio of populations in the L and Γ* states $n_{\mathrm{L}}/n_{\Gamma*}$. Typically, $n_{\mathrm{L}} \gg n_{\Gamma*}$ and the low fraction of carriers in the Γ* state constitutes a bottleneck for the carrier cooling [21] as it is also expressed by the above expression for T_y.

Given the relation between the effective masses [19]: $m_\Gamma \approx m_{\Gamma*}/2 \approx m_{\mathrm{L}}/7$ we can assess that in the total conductivity the contribution of Γ electrons is dominant and that of L-valley electrons is virtually negligible. We find experimentally that the initial increase in the pump–probe signal becomes faster upon increasing the irradiation dose. Indeed, the phonon scattering rates and the deformation potential for intervalley coupling could be altered owing to the host atom displacement defects. It appears that by increasing the irradiation dose one shortens T_y, i.e. τ_2 and τ_3 are shortened compared with τ_1. By fitting the pump–probe scans for samples A, B and C we cannot distinguish whether τ_2, τ_3 or both are shortened; however, the sub-picosecond data obtained for sample D (shown in section 3.3) suggest that the shortening of τ_2 is substantial. Taking the estimations for $\tau_1 = 35$ fs and $\tau_3 = 200$ fs from [21], our fits of the exact solution of equation (1) to the experimental results yield $\tau_2 = 440$ fs, 380 fs and 220 fs for samples A, B and C, respectively.

3.2. Electron transport and capture

The electron transport mechanism was deduced from the spectrally resolved transient conductivity measured at various pump–probe delays. Since, for samples A–C, the dynamics are substantially slower than the probing THz pulse duration, the transient conductivity is proportional to the ratio of the transient THz spectrum $\Delta E(f, \tau_{\mathrm{p}})$ transmitted through the sample and a reference THz spectrum $E_0(f)$ acquired with pump beam off: $\Delta\sigma(f, \tau_{\mathrm{p}}) \propto \Delta E(f, \tau_{\mathrm{p}})/E_0(f)$ [17]. The measured transient conductivity spectra are shown in figure 3. We found that the spectra of samples A, B and C for $\tau_{\mathrm{p}} \gg \tau_{\mathrm{rise}}$ can be well described by a single component representing the Drude response of free electrons:

$$\Delta\sigma(f, \tau_{\mathrm{p}}) = \frac{n_0 e_0^2}{m_{\mathrm{eff}}} \frac{\tau_{\mathrm{s}}}{1 - 2\pi \mathrm{i} f \tau_{\mathrm{s}}} \exp\left(-\tau_{\mathrm{p}}/\tau_{\mathrm{c}}\right). \tag{2}$$

Here n_0 is the initial electron density decaying with the lifetime τ_{c}, τ_{s} is their momentum relaxation time and e_0 is the elementary charge. The term $\mu_0 = e_0\tau_{\mathrm{s}}/m_{\mathrm{eff}}$ then expresses the photocarrier mobility (with $m_{\mathrm{eff}} = 0.041 m_{\mathrm{e}}$ being the effective mass of carriers [19]). Fitting the transient conductivity spectra with the Drude term allows determination of τ_{s} and, consequently, of μ_0.

3.3. Sub-picosecond dynamics

The dynamics in the most irradiated sample (D) are very fast compared with the THz pulse duration; therefore the simple analysis used for samples A–C cannot be applied; it is also impossible to separate in time the intervalley scattering from the carrier capture process. Our experimental data were analysed by using the kinetic model (1) and by assuming the Drude response of electrons [17]. We followed an approach based on the Fourier transformation into a two-dimensional frequency domain, which makes it possible to determine the transient photoconductivity $\Delta\sigma(f,\ f_{\mathrm{p}})$ analytically [23]. The frequency f_{p} is the Fourier-conjugated variable to the pump–probe delay τ_{p} and it describes the time evolution of the excited system towards equilibrium. The experimental procedure and data analysis are described in detail in [23].

The model involves several parameters, the most important of which for this study is the momentum relaxation time τ_{s} and the capture time τ_{c} of the Γ electrons. The (global) fitting of the complex conductivity in the $(f,\ f_{\mathrm{p}})$ plane then provides their values and also the intervalley scattering time $\tau_2/\tau_1 \approx 1$. This fit (figure 4) was done with the assumption that τ_3 is constant and the plot in figure 4 shows that there is an excellent match with the measured data within the experimentally accessible region of the $(f,\ f_{\mathrm{p}})$ plane. In contrast, if we keep τ_2 constant a roughly ten-fold reduction in τ_3 is found by fitting the experimental data while the residual sum of least squares for this fit is increased by about 20%. Finally, very poor agreement is obtained if both τ_2 and τ_3 are kept close to their value appropriate for as-grown samples ($\tau_2 \approx 350$ fs and $\tau_3 \approx 200$ fs). We conclude that the defects due to heavy-ion irradiation strongly modify the scattering rates, namely that for the intervalley scattering.

4. Discussion

The retrieved values of the electron lifetime are shown in figure 5. As expected, the decay time τ_{c} is inversely

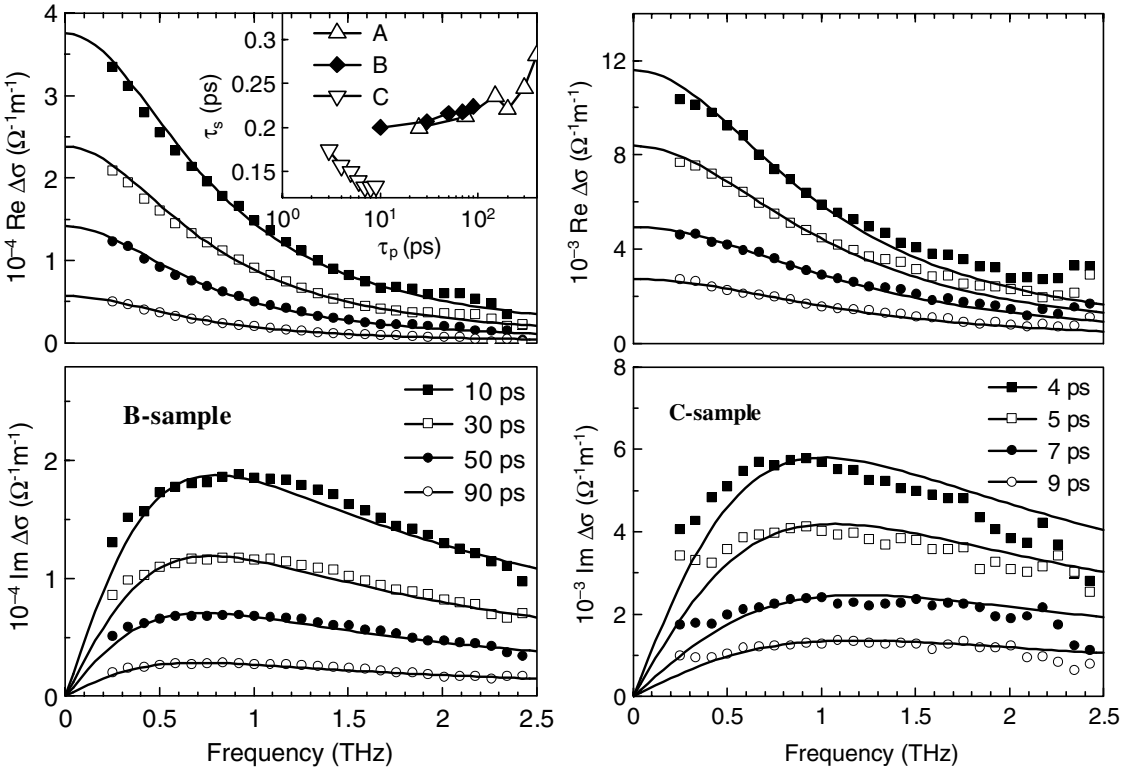

Figure 3. Spectra of real and imaginary part of transient conductivity $\Delta\sigma$ of the B- and C-sample for a few pump–probe delays τ_p. Points: experimental results, lines: fit using Drude formula (2). Inset: momentum relaxation times as a function of pump–probe delay in samples A, B and C.

proportional to the irradiation dose and it reaches 0.46 ps for an irradiation dose of $1 \times 10^{12}\,\mathrm{cm}^{-2}$. We observe somewhat longer lifetimes in comparison with those obtained by all-optical pump–probe experiments ([9]). The difference may be explained by the fact that the excitation wavelength used in those experiments was 1.55 μm. Thus, deeper parts of the InGaAs layers, containing higher density of defects, contribute to the signal and exhibit correspondingly shorter carrier lifetimes.

The ultrafast optoelectronic applications require high photocarrier mobility. Assuming that τ_s does not depend on the pump–probe delay we determined the average photocarrier mobilities on the ultrafast time scale for each of the samples (figure 5). It is noteworthy that in reality the momentum relaxation time τ_s slightly changes with τ_p. A small increase is observed in the A and B samples (see the inset of figure 3). We think that in these samples the electrons progressively lose their excess energy, and their momentum relaxation time thus slightly increases. In contrast, the observed decrease in τ_s in sample C may reflect the electron intervalley scattering, which is still occurring on the investigated time scale ($\tau_p < 7$ ps), and possibly also a non-vanishing population of the light holes at the early stages after photoexcitation.

The mobility in intrinsic InGaAs is very high due to the small electron effective mass [19]. Our experiments show that the photocarrier mobility remains relatively high even after heavy-ion irradiation. Its value for the C-sample is 50% higher than the electron Hall mobility reported in [9]. Further, in the most irradiated sample, we find $\mu_0 = 3600\,\mathrm{cm}^2\,\mathrm{V}^{-1}\,\mathrm{s}^{-1}$, which is an order of magnitude higher than the Hall mobility reported in [6, 9]. On the other hand, our values are in good agreement with the THz emission results discussed in [9]: the mobility values roughly estimated from the THz emission amplitude were $5400\,\mathrm{cm}^2\,\mathrm{V}^{-1}\,\mathrm{s}^{-1}$ for the sample nominally equivalent to our sample C and $2700\,\mathrm{cm}^2\,\mathrm{V}^{-1}\,\mathrm{s}^{-1}$ for the sample nominally equivalent to D.

It is rather frequent to find the drift or Hall mobility values smaller than the mobility of photoexcited carriers in damaged or disordered samples [17, 24]. This is related to the different nature of these quantities: the mobility of photoexcited carriers appears as a local response function of mobile carriers while the Hall and drift mobilities characterize macroscopic long-range and time-averaged transport which can be limited by carrier captures and releases and scattering on defect centres. The key quantity determining the performance of ultrafast optoelectronic elements is the high local mobility of photoexcited electrons. Its very high values observed in our experiments exceed those in other semiconductor materials exhibiting comparable capture times such as ion-irradiated InP or LTG GaAs [11, 25, 26].

As pointed out above, the observed high value of the photoexcited electron mobility is attributed to the electrons at the bottom of the Γ valley which yield a dominant contribution to the total photoconductivity. Such electrons can be directly excited by optical pulses at 1550 nm. Note that at this wavelength the penetration depth of the pump radiation is about 1.3 μm, which is smaller than the thickness of our GaInAs films [27]. However, the stopping range of Br ions is still higher than the penetration depth at 1550 nm (this claim stems directly from figure 1 in [11]). It then follows that (i) the contribution

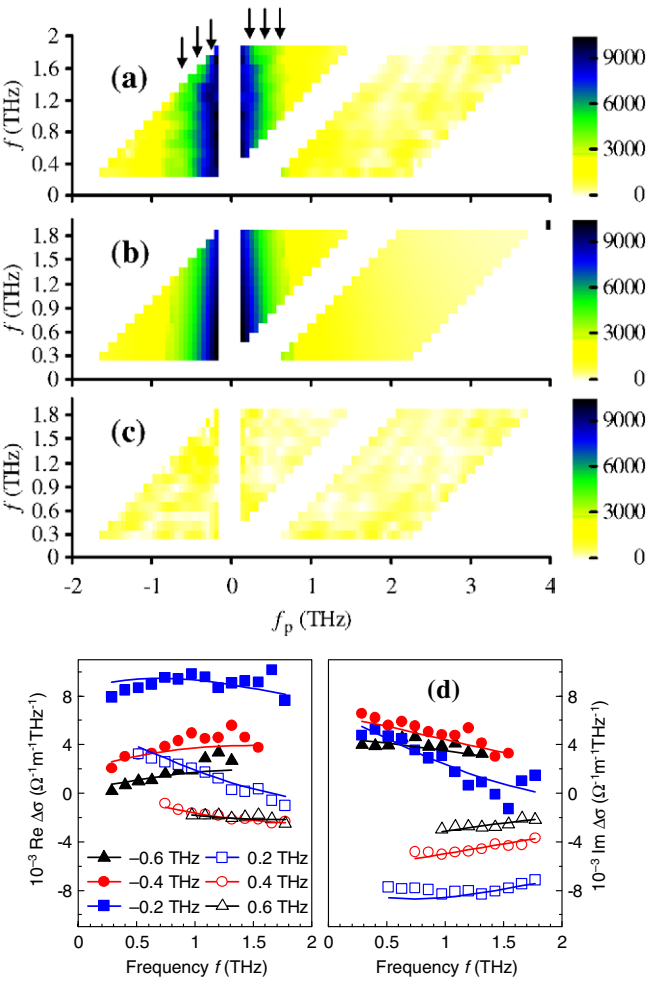

Figure 4. Transient conductivity of sample D. Amplitude of 2D spectra [Ω^{-1} THz^{-1} m^{-1}]: (*a*) experiment $|\Delta\sigma_{exp}(f, f_p)|$, (*b*) $|\Delta\sigma_{fit}(f, f_p)|$, (*c*) residual $|\Delta\sigma_{exp}(f, f_p) - \Delta\sigma_{fit}(f, f_p)|$; (*d*) cuts for several values of the frequency f_p of the real and imaginary part (symbols: experiment; lines: fit). The positions of the cuts are indicated by arrows in panel (*a*). (Colour online.)

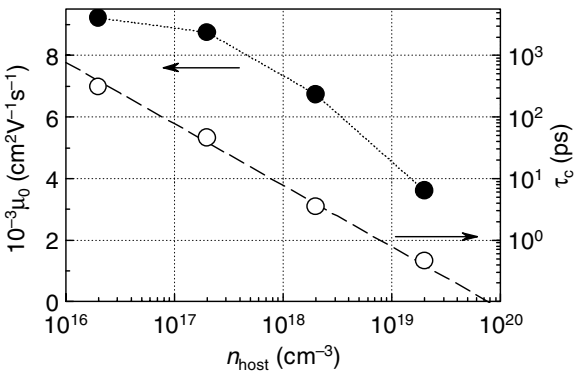

Figure 5. Photoexcited electron mobility (closed symbols) and electron capture time (open symbols) versus the density of host-atom displacements n_{host}. The trend $\tau_c \propto 1/n_{host}$ is shown as a dashed line.

of the substrate to the photoconductivity would be negligible and (ii) the motion of photocarriers would still occur in a layer virtually free of implanted Br ions. Taking into account these facts, we expect to obtain high electron mobility even with the photoexcitation in the telecommunication spectral range. Experiments in these conditions are in preparation.

5. Conclusion

We have investigated by optical pump–THz probe spectroscopy the transient conductivity in $In_{0.53}Ga_{0.47}As$ films irradiated by heavy high-energy ions. The electron capture rate is proportional to the density of host-atom displacement defects. The electron mobility is reduced upon high irradiation doses; nevertheless, an exceptionally high photoexcited electron mobility of 3600 cm^2 V^{-1} s^{-1} is found even in the most irradiated sample which exhibits a lifetime of 460 fs. This study demonstrates the large tunability of optical and electronic material parameters in ion-irradiated InGaAs and gives information for the improvement of ultrafast optoelectronic devices based on this material.

Acknowledgment

The financial support by the Czech Science Foundation (Project No 202/09/P099) and by ASCR and its Grant Agency (Projects No. AVOZ10100520 and A100100902) is acknowledged.

References

[1] Uhd Jepsen P, Jacobsen R H and Keiding S R 1996 *J. Opt. Soc. Am.* B **13** 2424
[2] Mangeney J, Joulaud L, Crozat P, Lourtioz J-M and Decobert J 2003 *Appl. Phys. Lett.* **83** 5551
[3] Suzuki M and Tonouchi M 2005 *Appl. Phys. Lett.* **86** 051104
[4] Takazato A, Kamakura M, Matsui T, Kitagawa J and Kadoya Y 2007 *Appl. Phys. Lett.* **90** 101119
[5] Carmody C, Tan H H, Jagadish C, Gaarder A and Marcinkevičius S 2003 *Appl. Phys. Lett.* **82** 3913
[6] Azad A K, Prasankumar R P, Talbayev D, Taylor A J, Averitt R D, Zide J M O, Lu H, Gossard A C and O'Hara J F 2008 *Appl. Phys. Lett.* **93** 121108
[7] Mangeney J, Chimot N, Meignien L, Zerounian N, Crozat P, Blary K, Lampin J F and Mounaix P 2007 *Opt. Express* **15** 8943
[8] Mangeney J and Crozat P 2008 *C. R. Phys.* **9** 142
[9] Chimot N, Mangeney J, Joulaud L, Crozat P, Bernas H, Blary K and Lampin J F 2005 *Appl. Phys. Lett.* **87** 193510
[10] Chimot N, Mangeney J, Mounaix P, Tondusson M, Blary K and Lampin J F 2006 *Appl. Phys. Lett.* **89** 083519
[11] Němec H, Fekete L, Kadlec F, Kužel P, Martin M, Mangeney J, Delagnes J C and Mounaix P 2008 *Phys. Rev.* B **78** 235206
[12] Hegmann F A, Ostroverkhova O and Cooke D G 2006 Probing organic semiconductors with terahertz pulses *Photophysics of Molecular Materials* (New York: Wiley) chapter 7 pp 367–428
[13] Biersack J P and Haggmark L G 1980 *Nucl. Instrum. Methods* **174** 257
[14] Joulaud L, Mangeney J, Lourtioz L M, Crozat P and Patriarche G 2003 *Appl. Phys. Lett.* **82** 856
[15] Joulaud L, Mangeney J, Chimot N, Crozat P, Fishman G and Bourgoin J C 2005 *J. Appl. Phys.* **97** 63515
[16] Mangeney J, Stelmakh N, Aniel F, Boucaud P and Lourtioz J-M 2002 *Appl. Phys. Lett.* **80** 4711
[17] Fekete L, Kužel P, Němec H, Kadlec F, Dejneka A, Stuchlík J and Fejfar A 2009 *Phys. Rev.* B **79** 115306

[18] Němec H, Kadlec F and Kužel P 2002 *J. Chem. Phys.* **117** 8454–66
[19] Levinshtein M, Rumyantsev S and Shur M (ed) 1999 Handbook Series on Semiconductor Parameters vol 2 (Singapore: World Scientific)
[20] Stanton C J and Bailey D W 1992 *Phys. Rev.* B **45** 8369
[21] Ralph S E, Chen Y, Woodall J and McInturff D 1996 *Phys. Rev.* B **54** 5568
[22] Beard M C, Turner G M and Schmuttenmaer C A 2000 *Phys. Rev.* B **62** 15764
[23] Němec H, Kadlec F, Kadlec C, Kužel P and Jungwirth P 2005 *J. Chem. Phys.* **122** 104504
[24] Lui K P H and Hegmann F A 2003 *J. Appl. Phys.* **93** 9012
[25] Němec H, Pashkin A, Kužel P, Khazan M, Schnüll S and Wilke I 2001 *J. Appl. Phys.* **90** 1303–6
[26] Gupta S, Frankel M Y, Valdmanis J A, Whitaker J F, Mourou G A, Smith F W and Calawa A R 1991 *Appl. Phys. Lett.* **59** 3276
[27] Zielinski E, Schweizer H, Streubel K, Eisele H and Weimann G 1986 *J. Appl. Phys.* **59** 2196